Nuclear Science and Techniques (2025) 36:59
https://doi.org/10.1007/s41365-024-01627-7

# A thermal–hydraulic model for the graphite-moderated channel-type molten salt reactor

Long He[1] · Jia-Jie Shen[1] · Xiang-Zhou Cai[2,3]

Received: 20 February 2024 / Revised: 24 June 2024 / Accepted: 14 July 2024 / Published online: 23 February 2025


## Abstract

A thermal–hydraulic model was developed to analyze the three-dimensional (3D) temperature field of a graphite-moderated channel-type molten salt reactor (GMC-MSR). This model solves the temperature distribution of both the graphite moderator and fuel salt using a single convection–diffusion equation. Heat transfer at the interface between the fuel salt and graphite was addressed by introducing an additional thermal resistance component at the interface and modifying the anisotropic thermal conductivity of the fuel salt. The mass flow distribution in different flow passages was determined by adjusting the mass flow rate until a uniform pressure drop was achieved across all fuel channels. This thermal–hydraulic model, constructed on COMSOL Multiphysics, was verified by comparing its temperature results with those from the RELAP5 code across two demonstration cases. A steady-state thermal–hydraulic simulation of this model was performed to evaluate the conceptual design of a 2-MW experimental molten salt reactor (2MW-MSR). In addition, detailed discussions of the 3D temperature field, heat flux, and mass flow distribution of the 2MW-MSR were presented. This model allows for a comprehensive 3D thermal–hydraulic analysis of the GMC-MSR. Moreover, it only requires the solution of a single convection–diffusion equation, which makes it invaluable for GMC-MSR design.

**Keywords** Molten salt reactor · Thermal–hydraulic analysis · Thermal coupling

## 1 Introduction

A graphite-moderated channel-type molten salt reactor (GMC-MSR) utilizes molten salt as fuel and graphite as the moderator. The reactor core is composed of regularly arranged graphite stringers or blocks. Fuel channels are formed either by the orderly arrangement of graphite stringers or by small cylindrical cavities present in the graphite blocks. Molten salt, which contains fissionable materials, fills the fuel channel and circulates within it. Self-sustained fission occurs within the molten salt only when it passes through the fuel channels shaped by the graphite moderator. A prime example of a GMC-MSR is the molten salt reactor experiment (MSRE), which was constructed and operated by the Oak Ridge National Laboratory (ORNL) in the 1960 s [1]. The MSRE was operated at 1200 °F and achieved a maximum operational power of 8 MW. The primary loop of the MSRE comprises a reactor vessel, a main pump, a heat exchanger, and an interconnected piping system. The reactor core contains 1140 equivalent fuel channels formed by graphite stringers [2]. In 4.5 years, the MSRE successfully demonstrated and established key technologies for an MSR [3]. The 2002 Generation IV roadmap declared MSR as a candidate for next-generation reactors owing to its high operating temperature, negative fuel salt temperature coefficient, and the Th-U breeding and actinide transmuting capabilities [4]. In January 2011, a Th-based MSR project was initiated by the Shanghai Institute of Applied Physics (SINAP), Chinese Academy of Sciences, aiming to build a small MSR and master the technology of efficiently utilizing Th resources

This work was supported by the National Natural Science Foundation of China (No.12075169).

✉ Long He
helong@shmtu.edu.cn

[1] School of Science, Shanghai Maritime University, Shanghai 201306, China

[2] Shanghai Institute of Applied Physics, Chinese Academy of Sciences, Shanghai 201800, China

[3] University of Chinese Academy of Sciences, Beijing 100049, China

[5, 6]. In recent years, the SINAP has conducted extensive research on various aspects of MSRs, including thermal neutron scattering data [7], reliability of the core fuel salt emergency drain system [8], optimal hydraulics design [9], impact of graphite structures on reactivity [10], and incineration characteristics of transuranic nuclides in a small modular chloride fast reactor [11].

The GMC-MSR, which utilizes a liquid salt mixture as fuel, demonstrates distinct thermal–hydraulic behavior compared with traditional solid-fueled reactors. In the GMC-MSR, the liquid salt mixture serves both as coolant and fuel. Consequently, fission energy is primarily released into salt. The flowing salt promptly carries it away, leading to improved heat-transfer characteristics. Fuel salt also has a higher volumetric heat capacity than water and gaseous coolants, which enhances the system's ability to remove heat. A small portion of the fission energy generated by gamma and fast neutron radiation [12] is deposited in the graphite moderator and removed from the reactor core by the salt. In GMC-MSR, the moderator is cooled by the fuel salt, causing the moderator to have a higher temperature than the fuel. In GMC-MSR, each flow passage in the reactor core is isolated using graphite. Unlike the calculations for pressurized water reactors, the lateral flow between channels does not need to be considered in the thermal–hydraulic analysis of GMC-MSR. Therefore, in GMC-MSR, the thermal coupling of adjacent fuel assemblies is achieved through a graphite moderator via heat conduction. Due to the distinct features of GMC-MSR, its thermal–hydraulic analysis presents significantly more challenges than that of solid fuel reactors, given that most extant models are primarily designed for solid fuel reactors.

The reactor core of GMC-MSR constitutes numerous fuel assemblies, each with a hexagonal or square cross section. Currently, three primary methods are used for the thermal–hydraulic analysis of GMC-MSRs. The first method omits thermal coupling between these fuel assemblies and employs a one-dimensional (1D) heat conduction model to calculate the temperature of the moderator. In addition, a 1D single-phase flow model is used to simulate the behavior of fuel salt within the reactor. The fuel assembly is modeled as a hollow cylinder with equivalent fuel salt and graphite volume and height. Subsequently, the cylinder is divided into multiple nodes along the flow direction. The average temperature of the fuel salt and the 1D radial temperature of the graphite moderator within each node are calculated. The reactor core is represented by several equivalent hollow cylinders, each representing a region with a distinct energy distribution. The mass flow in each cylinder is determined by assuming an equal pressure drop across parallel channels. This method can be performed analytically or numerically, to capture the essential thermal–hydraulic characteristics of GMC-MSR. However, it does not consider the conductive heat flux between different assemblies or provide the temperature distribution of the reflector. Therefore, it is not suitable for the case of strong thermal coupling between fuel assemblies, such as during channel blocking or when the fuel assembly is close to the control rod or reflector. Engel et al. used this method to analytically calculate the fuel salt and graphite temperatures for an MSRE [13]. Zhang et al. employed this model to investigate the steady-state thermal–hydraulic characteristics of MSRs [14]. Guo et al. adopted this model and coupled it with a neuronic code to optimize the design of MSRs [15]. The thermal–hydraulic model described above has been adopted in several dynamic codes for GMC-MSR, including 1D codes Cinsf1D [16], TREND [17] and TRACE [18], two-dimensional code TMSR-2D [19, 20], and three-dimensional (3D) codes DYN3D-MSR [21], MOERL [22, 23], ThorCORE3D [24], TMSR3D [25], and TANG-MSR [26]. The second method considers thermal coupling between the fuel assemblies and the reflector. The reactor core of GMC-MSR is described as a large graphite block with regularly distributed channels. This method utilizes a 3D heat conduction equation to calculate the moderator temperature and a 1D heat convection equation to represent the fuel salt in each channel. Thermal coupling between graphite and fuel salt has been established by utilizing heat transfer coefficients at the solid–liquid interface. He et al. established a mathematical model based on COMSOL Multiphysics software and MATLAB software and applied it to the steady-state and dynamic analysis of a small experimental GMC-MSR [27, 28]. Representative dynamic codes that have adopted this thermal–hydraulic model include DT-MSR [29], Moltres [30], and the code developed by Nagy [31]. This thermal–hydraulic model accurately captures the heat transfer characteristics of the GMC-MSR and provides 3D temperature profiles of the reactor core and reflector. In general, it employs structured grids to simulate heat conduction in graphite and requires the cross section of the channel to be equivalent to a rectangle. However, when modeling a GMC-MSR with numerous fuel channels, identifying the solid–liquid interface and inputting the heat transfer coefficients for each channel can be cumbersome. The third method involves utilizing computational fluid dynamics (CFD) to analyze the temperature and velocity distributions of either the entire reactor core or a specific region thereof. This method constructs 3D computational domains for both graphite and fuel salt with minor geometric approximations. Finally, it solves the Navier–Stokes equation, the transport equation for the turbulence model, and the energy equation within these domains. He et al. from Shanghai Institute of Applied Physics utilized Fluent to analyze the temperature and flow characteristics of a 2-MW GMC-MSR [32]. Cammi et al. analyzed the

velocity and temperature fields within a single-fuel assembly of a molten salt breeder reactor using the CFD module of COMSOL Multiphysics [33].

This study introduces a 3D steady-state thermal–hydraulic model named 3DSTH-MSR for the GMC-MSR to simplify the thermal–hydraulic analysis of this reactor. The rest of the paper is organized as follows. Section 2 presents mathematical equations and verifying the 3DSTH-MSR model. Section 3 details the calculations of temperature and mass flow distributions in the 2-MW experimental MSR using the 3DSTH-MSR model, along with a comprehensive analysis of the results.

## 2 Numerical model and verification

### 2.1 Thermal hydraulics model

In the 3DSTH-MSR, the temperature field within the reactor core of the GMC-MSR, which encompassed the graphite assemblies, reflector, and liquid region, was calculated using a 3D convection–diffusion equation:

$$\frac{\partial(\rho C_p uT)}{\partial x}+\frac{\partial(\rho C_p vT)}{\partial y}+\frac{\partial(\rho C_p wT)}{\partial z} = \frac{\partial}{\partial x}\left(\lambda_{xx}\frac{\partial T}{\partial x}\right)+\frac{\partial}{\partial y}\left(\lambda_{yy}\frac{\partial T}{\partial y}\right)+\frac{\partial}{\partial z}\left(\lambda_{zz}\frac{\partial T}{\partial z}\right)+Q, \tag{1}$$

where $\rho$, $u$, $v$, $w$, $C_p$, $Q$, and $T$ are the density, $x$-, $y$-, and $z$-components of the velocity vector, specific heat capacity at constant pressure, heat source, and temperature, respectively. Thermal conductivity $\lambda$ is expressed in the tensor form, which is a symmetric matrix.

$$\lambda=\begin{bmatrix}\lambda_{xx} & 0 & 0\\ 0 & \lambda_{yy} & 0\\ 0 & 0 & \lambda_{zz}\end{bmatrix} \tag{2}$$

where $\lambda_{xx}$, $\lambda_{yy}$ and $\lambda_{zz}$ represent the $xx$, $yy$, and $zz$ components of tensor $\lambda$, respectively. For the solid region, isotropic thermal conductivity was employed, where $\lambda_{xx}=\lambda_{yy}=\lambda_{zz}$. However, in the liquid region, anisotropic thermal conductivity is utilized. Equation (1) neglects the contributions of viscous dissipation, pressure work, and kinetic energy.

Within the solid region, $u$, $v$, and $w$ were each set to zero, leading to the transformation of Eq. (1) into a heat conduction equation with an internal heat source.

$$\frac{\partial}{\partial x}\left(\lambda_{xx}\frac{\partial T}{\partial x}\right)+\frac{\partial}{\partial y}\left(\lambda_{yy}\frac{\partial T}{\partial y}\right)+\frac{\partial}{\partial z}\left(\lambda_{zz}\frac{\partial T}{\partial z}\right)+Q=0 \tag{3}$$

To obtain a 1D fuel-salt temperature profile along flow direction $z$ for each channel, the $\lambda_{xx}$ and $\lambda_{yy}$ components of thermal conductivities in the 3DSTH-MSR were assigned infinite values ($1\times10^6$ W/(m·K)) in the 3D liquid region. Because we set $\lambda_{xx}$ and $\lambda_{yy}$ to infinitely large quantities, the $x$ and $y$ components of temperature gradients ($\frac{\partial T}{\partial x}$ and $\frac{\partial T}{\partial y}$) tended to zero. This led to a nearly uniform distribution of the fuel-salt temperature within each channel along the direction perpendicular to the flow. In addition, the fuel-salt temperature profile of each channel was affected by the $z$-component of the temperature gradient.

To describe the heat convection along the $z$ direction, velocity components $u$ and $v$ were set to zero, while the $z$-component of velocity $w$ was set as

$$w=\frac{m_{\text{flow}}}{\rho(T)\cdot A}, \tag{4}$$

where $m_{\text{flow}}$ and $A$ denote the mass flow and cross-sectional area of the fuel channel, respectively. $\rho(T)$ denotes the density of fuel salt, which is a function of temperature. The $z$-component of velocity $w$ was updated after each iteration of the temperature calculation. By modifying the conductivity and velocity in the 3D liquid region, Eq. (1) yields a 1D fuel-salt temperature profile along the flow direction, similar to that of the 1D heat convection equation.

Thermal coupling between the solid and liquid regions was established by adding thermal resistance at the solid–liquid interface, as shown in Fig. 1a. Thermal resistance causes temperature discontinuities at the interface, as shown in Fig. 1b. The heat flux at the solid–liquid interface can be written as

$$q=\frac{\Delta T}{R}, \tag{5}$$

where $q$, $\Delta T$, and $R$ represent the heat flux, temperature difference at the solid–liquid interface, and specific thermal resistance, respectively. The specific thermal resistance is related to the convective heat transfer coefficient and Nusselt number using the following equation:

$$h=\frac{Nu\cdot\lambda_{zz}}{D}=\frac{1}{R}, \tag{6}$$

where $h$, $Nu$, and $D$ are the convective heat transfer coefficient, Nusselt number, and hydraulic diameter of the fuel channel, respectively. $Nu$ was calculated based on a forced-convection heat-transfer experiment conducted by ORNL. The fitted empirical correlation for the laminar flow has the following form [34]:

$$Nu=1.89\left(Re\cdot Pr\cdot\frac{D}{L}\right)^{0.33}\left(\frac{\mu_l}{\mu_s}\right)^{0.14}, \tag{7}$$

where $Re$, $Pr$, $L$, $\mu_1$, and $\mu_s$ represent the Reynolds number, Prandtl number, fuel channel length, dynamic viscosities calculated using the liquid temperature, and dynamic

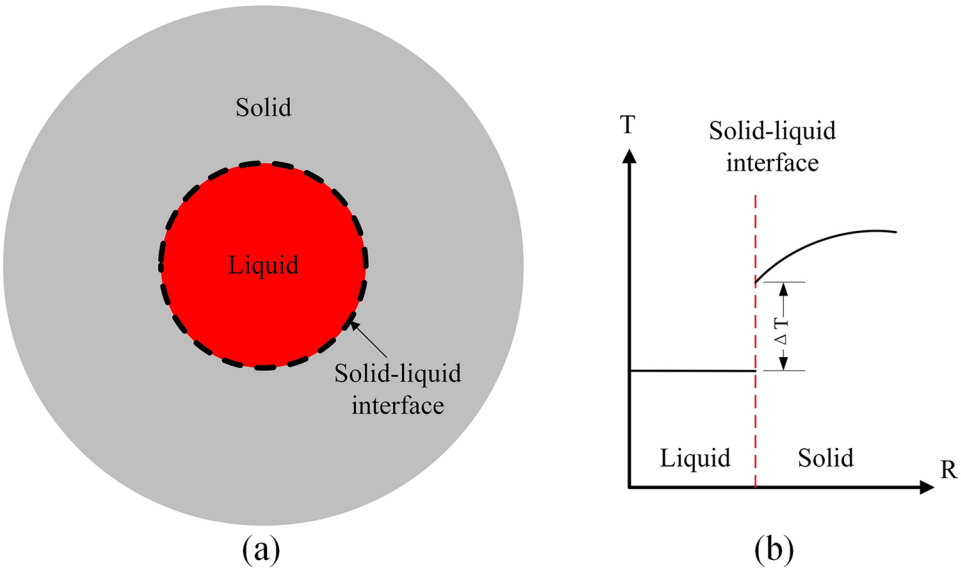


**Fig. 1** The sketch maps of solid–liquid coupling interface **a** and the temperature profile **b**

viscosity calculated using the solid surface temperature, respectively.

After imposing thermal resistance at the solid–liquid interface and modifying $\lambda_{xx}$ and $\lambda_{yy}$ for the liquid region, the radial temperature profile of the fuel assembly was similar to that shown in Fig. 1b. In the 3DSTH-MSR, the adiabatic boundary condition was applied to the outer walls of the solid region, while the temperature boundary condition was set at the inlet of the liquid region.

The pressure losses due to gravity, friction, localized effects, and acceleration effects in the $i_{\text{th}}$ channel are calculated using the following equations:

$$\Delta P_{\text{g},i} = \frac{1}{A_i} \iiint \rho g \mathrm{d}x\mathrm{d}y\mathrm{d}z, \tag{8}$$

$$\Delta P_{\text{f},i} = \frac{1}{A_i} \iiint f \frac{\rho}{2D_i} \left( \frac{m_{\text{flow},i}}{\rho \cdot A_i} \right)^2 \mathrm{d}x\mathrm{d}y\mathrm{d}z, \tag{9}$$

$$\Delta P_{\text{k},i} = \frac{k}{A_i} \iint \frac{\rho}{2} \left( \frac{m_{\text{flow},i}}{\rho \cdot A_i} \right)^2 \mathrm{d}x\mathrm{d}y, \tag{10}$$

$$\Delta P_{\text{a},i} = \frac{m_i}{A_i}(w_{\text{o}} - w_i), \tag{11}$$

where $g$, $f$, $k$, $w_{\text{o}}$, and $w_i$ represent the acceleration due to gravity, friction factor, coefficient of resistance, and $z$ component of the velocity vector at the channel outlet and inlet, respectively. Subscripts $g$, $f$, $k$, and $a$ represent the gravitational, frictional, local, and acceleration pressure drops, respectively. Total pressure drop $\Delta P_{\text{t},i}$ for the $i_{\text{th}}$ channel is defined as

$$\Delta P_{t,i} = \Delta P_{g,i} + \Delta P_{f,i} + \Delta P_{k,i} + \Delta P_{a,i}. \tag{12}$$

The mass flow in different fuel channels was determined by adjusting the mass-flow distribution until a uniform pressure drop was attained across all the fuel channels.

Figure 2 illustrates the computational procedure for the 3DSTH-MSR. First, in the initialization stage, uniform flow rate and temperature distribution were established. These initial conditions were utilized to calculate the $z$-components of velocity and thermal resistance. Subsequently, Eq. (1) was solved to obtain the temperature distribution. The pressure drops for each channel are updated based on the solution of Eq. (1). Subsequently, the flow distribution was readjusted based on these updated pressure drops, initiating a new iteration of the calculation process. This iterative procedure was repeated until convergence, which ultimately provided the desired solution. The computational procedure of 3DSTH-MSR method, as shown in Fig. 2, is implemented on COMSOL Multiphysics [35]. The Heat Transfer module of COMSOL was used to calculate the temperature distribution in both the solid and liquid phases. The MATLAB interface in COMSOL was employed to extract the pressure drop values and reset the mass flow distribution for the subsequent iteration of the temperature calculation. The 3DSTH-MSR can perform calculations on complex topologies using either structured or unstructured meshes.

It treats the liquid and solid domains as a collection of geometric objects. In the process of constructing the geometric model, COMSOL automatically detected the interfaces between the solid and liquid domains and established contact pairs to ensure appropriate contact between

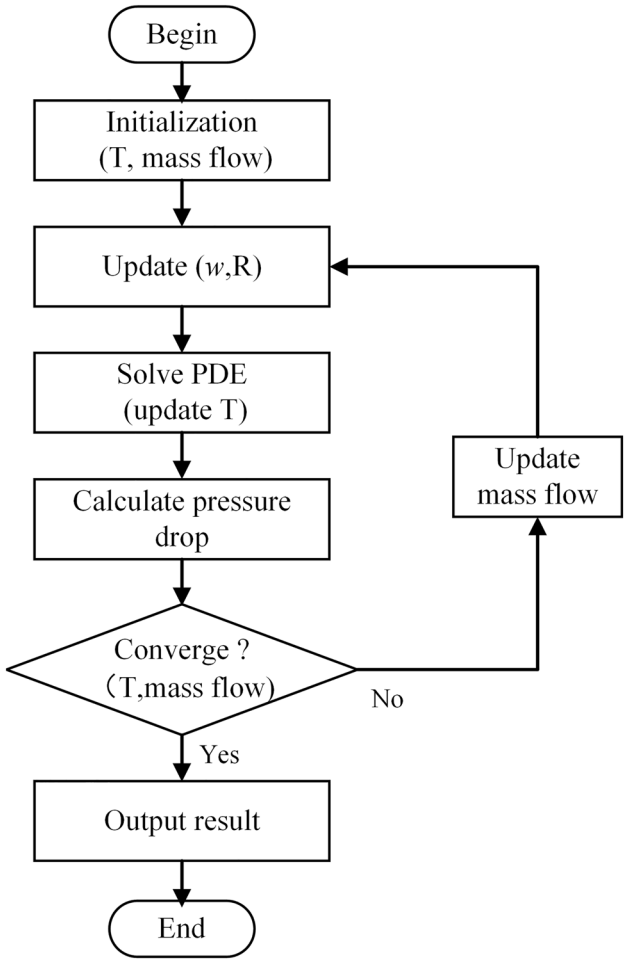


**Fig. 2** Flow chart of 3DSTH-MSR

them. Heat flux, described by Eq. (5), was implemented by applying thermal resistance $R$ at these contact pairs, which allowed coupling of the 3D solid temperature with the liquid temperature. The 3DSTH-MSR required only the solution of a 3D convection–diffusion equation, enabling efficient and automatic thermal coupling between various solid and liquid interfaces. This distinctive characteristic not only yielded substantial reductions in computational time compared with conventional CFD methods, but also eliminated the need for supplementary procedures to couple the 3D solid temperature with the 1D liquid temperature.

### 2.2 Verification of 3DSTH-MSR

The 3DSTH-MSR model developed in this study for GMC-MSR consisted of two primary components. The first component of the model involved the utilization of a single partial differential equation to derive the temperature distributions of both graphite and molten salt. The second component was grounded in the principle of equal pressure drop to ascertain the flow distribution within each flow channel. Regarding the validation of the second part, because it utilized a widely applicable flow-distribution calculation approach, this model has already been employed and verified in a previous study [36]. To verify the temperature field computed using the 3DSTH-MSR model, we employed the RELAP5 code [37].

To verify the program, a circular pipe cooled by a coolant was selected as the simulation object. The pipe had a length of 0.6 m, an inner diameter of 0.02 m, and a wall thickness of 0.01 m. We used FLiBe as the coolant. The thermal conductivity of the pipe wall material was 20 W/(m · K). For the boundary conditions, the inlet mass flow rate of the pipe was set to 0.5 kg/s, and the corresponding inlet temperature was 873.15 K. The total thermal power within the pipe was 23860.0 W. Notably, under these operating conditions, the Dittus–Boelter equation was utilized to calculate the Nusselt number for turbulent flow in both the 3DSTH-MSR and RELAP5 simulations. Due to the thermal power distribution in the GMC-MSR being different from that in traditional reactors, two distinct cases, Cases A and B, were considered. In Case A, 90% of the thermal power was uniformly deposited in the coolant, with the remaining portion being uniformly deposited along the tube wall. In Case B, the opposite configuration was used. For the calculation of the solid region temperature, the RELAP5 code utilized a 1D heat conduction model, disregarding heat conduction along the direction of coolant flow. The conductive heat flux in the axial direction can be neglected because the tube wall was actively cooled.

To accurately verify the 3D temperature field calculated by the 3DSTH-MSR, its results and those obtained using RELAP5 were compared. Figures 3a and 4a compare the radial temperature profiles at five positions along the pipe for Cases A and B, respectively. These positions were selected sequentially from the bottom to the top of the pipe. The calculated coolant temperature (in the liquid region) and tube wall temperature (in the solid region) obtained from the 3DSTH-MSR corroborated those calculated using RELAP5. The 3D temperature profile of the pipe obtained using the 3DSTH-MSR for Cases A and B is shown in Figs. 3b and 4b. The verification calculations exhibited satisfactory agreement between the 3DSTH-MSR and RELAP5 code results, confirming the accuracy and reliability of 3DSTH-MSR.

## 3 Calculation model and results

This section focuses on the analysis of the steady-state thermal hydraulic characteristics of a 2MW experimental MSR (hereinafter referred to as 2MW-MSR) under normal operating conditions using the 3DSTH-MSR. The first part of

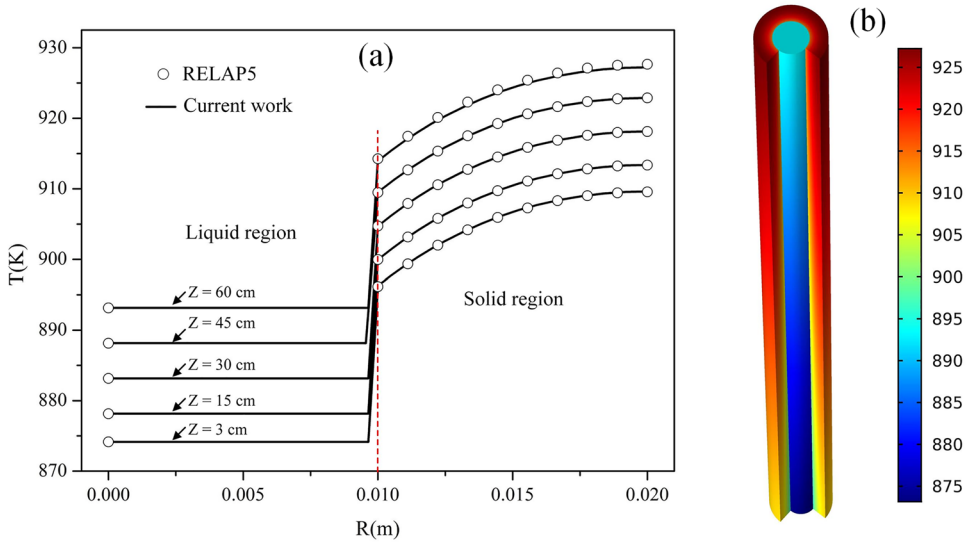


**Fig. 3** (Color online) Temperature distribution in Case A. **a** Radial temperature distribution in the pipe, **b** temperature profile of the pipe (unit: K)

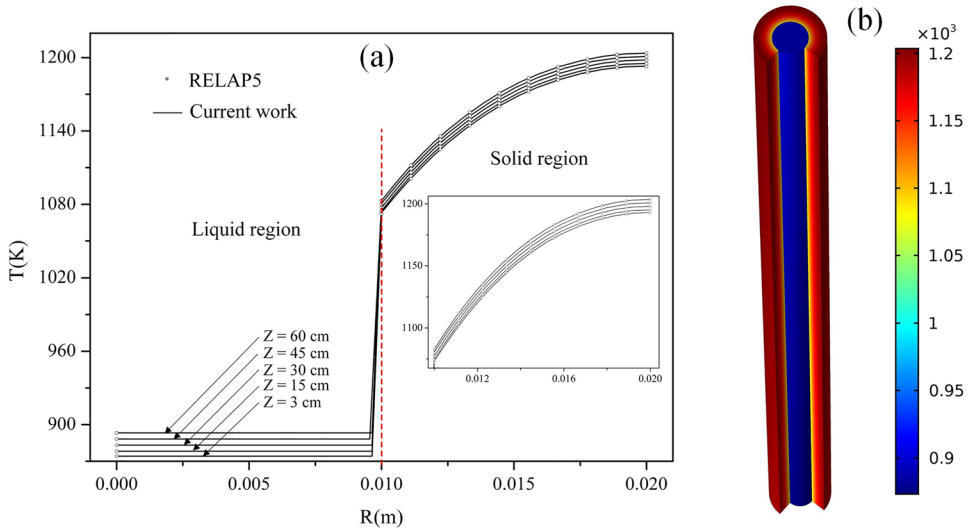


**Fig. 4** (Color online) Temperature distribution in Case B. **a** Radial temperature distribution in the pipe, **b** temperature profile of the pipe (unit: K)

this section provides a concise overview of the 2MW-MSR, while the subsequent part highlights the analysis results and discusses them.

### 3.1 2MW-MSR description

The 2MW-MSR is a small-scale experimental MSR designed by the Shanghai Institute of Applied Physics, Chinese Academy of Sciences. A schematic of the MSR and its dimensional parameters is illustrated in Fig. 5. The designed rated power and mass flow rate of the 2MW-MSR were 2 MW and 59.25 kg/s, respectively. The 2MW-MS was designed with an inlet temperature of 600 °C and an outlet temperature of 620 °C.

The reactor core comprises a block of graphite, which can be subdivided into 85 fuel assemblies, as shown in Fig. 5b. The fuel assembly had a hexagonal cross section with a circular fuel channel. Its dimensions are shown in Fig. 5c. The 2MW-MSR utilized graphite as its moderator, with Hastelloy-N alloy as the material for both the reactor vessel and structure. The thermophysical properties of graphite, Hastelloy-N alloy, and fuel salt are listed in Table 1 [36]. The graphite and the reactor vessel in the 2MW-MSR were separated by a 5-mm gap. A portion of the molten salt (the outer salt layer in Fig. 5a and b) flows through this gap, providing a cool environment for the reactor vessel.

The distribution of thermal power within the reactor core of the 2MW-MSR was calculated using the SCALE code [39] in previous research [28]. The results indicated that 65.68% of the thermal power was deposited in the fuel salt region of the assembly, while 3.39% was deposited in the graphite region of the assembly. Additionally, the fractions of thermal power deposited in the fuel salt within the bottom plenum, top plenum, and 5-mm gap were 11.25%, 12.50%,

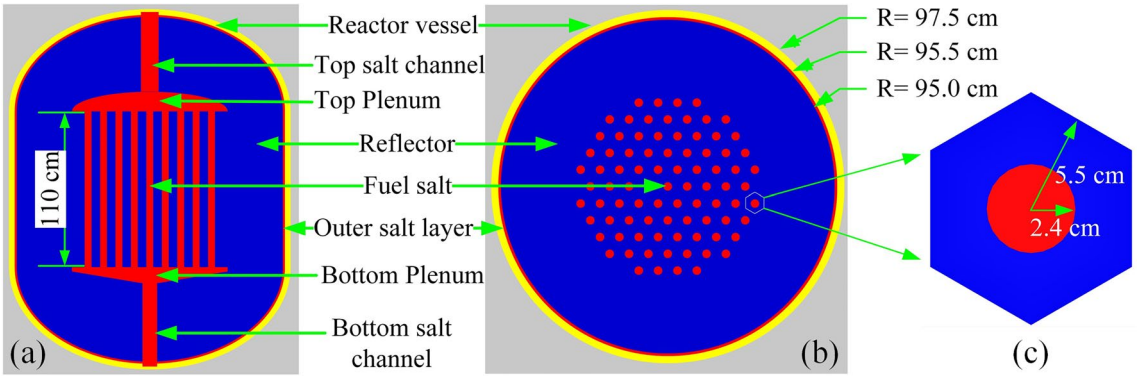


**Fig. 5** (Color online) Schematic of 2MW-MSR [38]. **a** Vertical cross section; **b** horizontal cross section; **c** cross section of the assembly

**Table 1** Material properties of the 2MW-MSR

| Parameter | Value |
|---|---|
| Graphite heat conductivity (W/(m · K)) | 60.49 |
| Hastelloy-N thermal conductivity (W/(m · K)) | 18.31 |
| Fuel salt composition (mol%) | 70.2 LiF−26.8 $BeF_2$ −0.073 $ThF_4$ −2.927 $UF_4$ |
| Fuel salt density (kg/m$^3$) | $3297.84 - 0.615832T$ |
| Fuel salt heat conductivity (W/(m · K)) | $0.3981 + 5 \times 10^{-5}T$ |
| Fuel salt dynamic viscosity (Pa · s) | 0.0094 |
| Fuel salt-specific heat capacity (J/(kg · K)) | 1687.89 |

and 4.41%, respectively. The remaining thermal power was released into the structural material and reflector components. Figure 6 depicts the 3D thermal power distribution for the simulation in our study. The impact of the drift of delayed neutron precursors (DNP) and decay heat on the thermal power distribution in the active core was disregarded. Zhang [40] obtained the neutron flux distribution in an MSR for various fuel velocities under steady-state conditions. They observed that the drift of delayed neutron precursors had a negligible impact on the neutron flux. Zhou [41] studied decay heat distribution in a comparable MSR. Their findings revealed that the decay heat released in the active core accounted for 46.7% of the total decay heat. The influence of the drift of the DNPs and delayed heat on the temperature distribution in the MSR was found to be negligible. This is because the delayed neutron contribution accounted for approximately 0.67% of the total neutron population, while the decay heat contributed approximately 7% of the total thermal power.

### 3.2 Results and discussion

The calculation model included all the assemblies, a radial reflector, and flowing salt in the 5-mm gap. However, the plenums and the top and bottom regions of the graphite reflectors were not included in the model. The flow rates in channels except for outer salt layer were calculated using the principle of equal total pressure drop in the 3DSTH-MSR. In addition, the flow rate in the outer salt layer was set to the designed value of 5% of the rated flow.

In the analysis, a free tetrahedral mesh was adopted. A grid independence test was conducted on the calculation model. Table 2 lists the maximum and average temperatures of graphite and fuel salt for different grid numbers. The results indicated that the temperature was not significantly affected by the increase in grid number beyond 0.82 million grids.

The temperature fields of the 2MW-MSR are shown in Fig. 7. Because the energy deposited in graphite was cooled by the flowing fuel salt, the graphite reached a higher temperature than the salt. However, because only a small fraction of the fission power is released in graphite and because of the excellent convective heat transfer coefficient between

**Table 2** Grid independence calculation

| Grid number ×10$^3$ | Maximum graphite Temperature (°C) | Average graphite Temperature (°C) | Maximum fuel Temperature (°C) | Average fuel Temperature (°C) |
|---|---|---|---|---|
| 5586.48 | 628.73 | 622.89 | 617.87 | 609.89 |
| 2473.12 | 628.73 | 622.89 | 617.88 | 609.89 |
| 820.55 | 628.75 | 622.90 | 617.88 | 609.89 |
| 314.73 | 629.53 | 623.40 | 619.06 | 610.46 |

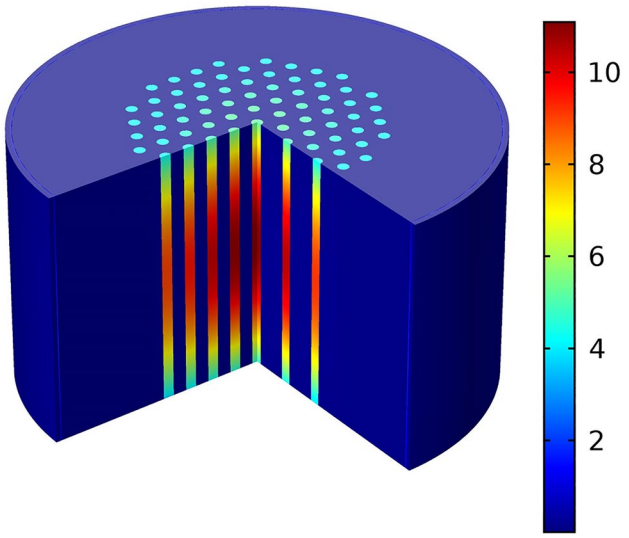


**Fig. 6** (Color online) Power density distribution in the 2MW-MSR (unit: MW/m$^3$)

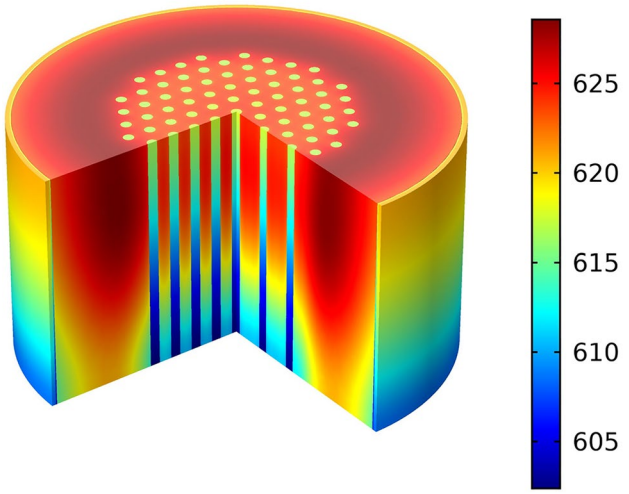


**Fig. 7** (Color online) Temperature distribution of 2MW-MSR (unit: °C)

the fuel salt and graphite, the temperature difference between the graphite and fuel salt is not significant. The maximum temperature reached in the 2MW-MSR was 628.7 °C, and it was located in the top region of the radial reflector.

The temperature distribution and isotherms at the horizontal cross section of the core at half height are presented in Fig. 8. The salt outer layer plays a crucial role in cooling the reflector adjacent to the reactor vessel, causing the reflector near the reactor vessel to have a lower temperature than that near the fuel assemblies. As depicted in Fig. 8b, the majority of isotherms within the inner region of the reactor core encircle the fuel channels. This observation suggests that most of the thermal energy generated in the graphite of each assembly was dissipated through the surrounding fuel salt within that assembly. Moreover, this pattern indicates insignificant thermal coupling between neighboring assemblies. The fuel assemblies located at the periphery of the core, along with the outer salt layer, play a vital role in dissipating the energy released in the radial reflector. The uniform cooling effect of the outer salt layer results in isothermal lines within the reflector adjacent to the reactor vessel, demonstrating a distinct circular shape and concentric circular distribution. Owing to the combined influence of the radial reflector and the cooling effect of the fuel assemblies, the isotherms near the reflector in the fuel assemblies exhibited noticeable deviations from a circular shape.

As part of the investigation of heat transfer characteristics of the 2MW-MSR, the conductive heat flux vectors in a 1/4 cross section at half the height of the core are depicted in Fig. 9. The lengths and directions of the vectors represent the magnitude and direction of heat transfer, respectively. Because the energy deposited in an assembly is primarily dissipated by the fuel salt within the same assembly, the heat flux vectors within an assembly point toward the center of the fuel channel. The conductive heat flux vectors in the reflector exhibit two distinct characteristics. When the radius is less than 0.63 m, the heat flux vectors point toward the center of the reactor. Conversely, when it exceeds 0.63 m, the vectors point outward. This phenomenon indicates that the energy deposited in the reflector within a radius of 0.63 m is primarily removed by the fuel assemblies, while the remaining energy deposited in the reflector is cooled by the outer salt layer.

The mass flow distribution in the reactor core of the 2MW-MSR is illustrated in Fig. 10. The highest mass flow of 0.73 kg/s was observed at the center of the reactor, while the lowest mass flow of 0.64 kg/s was observed in the fuel channel adjacent to the reflector. The mass flow calculation considered only the gravitational, frictional, and acceleration pressure drops. The local pressure drops at the top and bottom plenums caused by the presence of a distribution plate and changes in the flow section were not considered. Moreover, the density of the fuel salt decreases with increasing temperature; consequently, a greater mass flow was allocated to assemblies with higher energy deposition, and the mass flow distribution closely followed the power density profile.

Figure 11 depicts the salt outlet temperature in each fuel channel and the outer salt layer. As observed in the figure, the outlet temperature of the 2MW-MSR is relatively uniform, with a maximum deviation of approximately 1 °C. This is primarily attributed to the higher mass flow distribution in the fuel channels with higher fission energy. In this simulation, a designed mass flow value was specified for the outer salt layer. This layer not only removed 4.41% of the rated power deposited within it, but also effectively

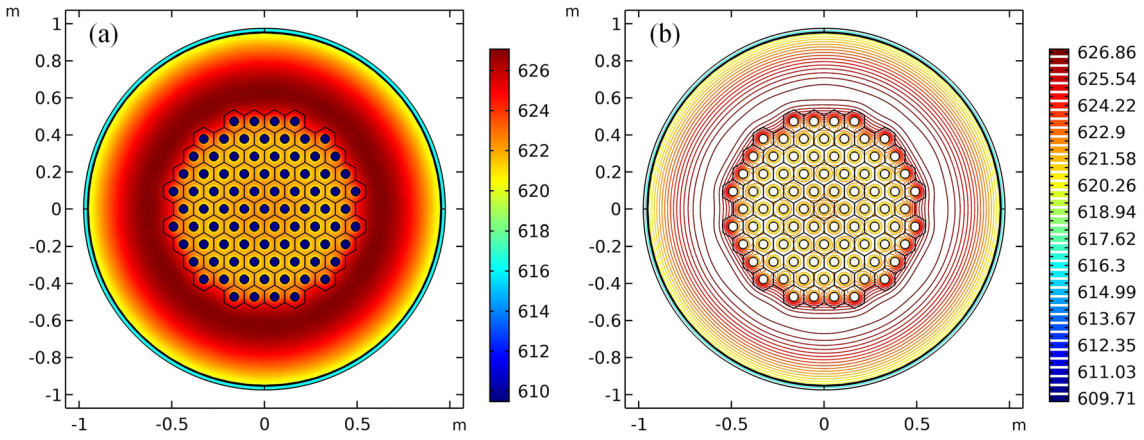


**Fig. 8** (Color online) Temperature field (**a**) and isotherm distribution (**b**) in cut plane $z = 0.55$ m (unit: °C)

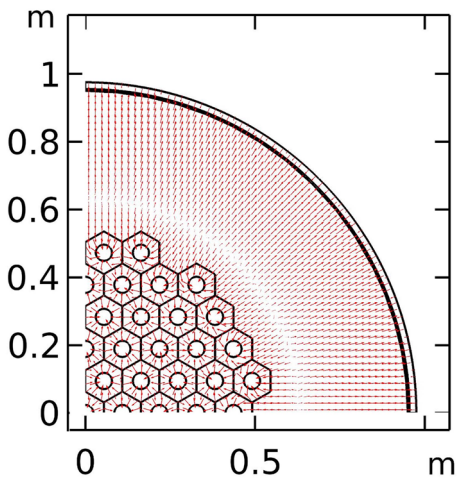


**Fig. 9** (Color online) The conductive heat flux vectors in the 1/4 cross section ($z = 0.55$ m)

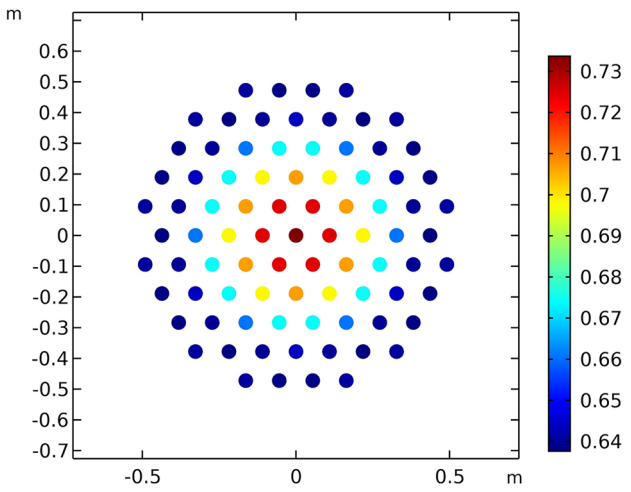


**Fig. 10** (Color online) The mass flow in each channel (unit: kg/s)

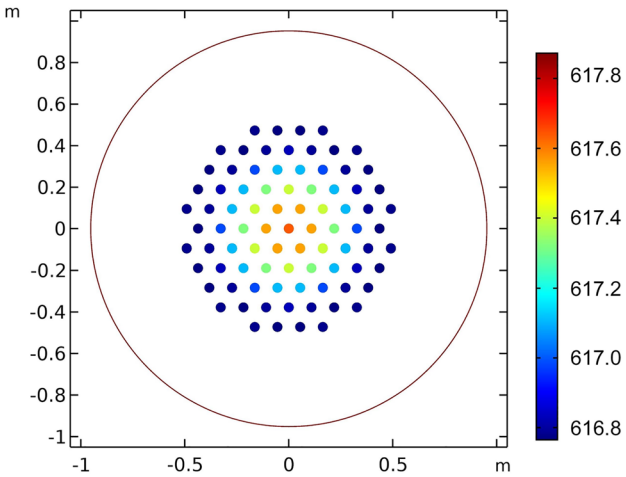


**Fig. 11** (Color online) The outlet fuel temperature (unit: °C)

dissipated most of the energy in the reflector region. In this design, the highest outlet temperature of the fuel salt was observed in the outer salt layer.

## 4 Summary

In this study, a thermal–hydraulic method, 3DSTH-MSR, was introduced for the steady-state analysis of GMC-MSR. The 3DSTH-MSR employed a 3D convection–diffusion equation to determine the temperature distribution in both the solid and liquid domains. The temperature distribution in the solid region was coupled with that in the liquid region by introducing thermal resistance at the solid–liquid interface. Additionally, anisotropic thermal conductivity was implemented in the liquid region, with $\lambda_{xx}$ and $\lambda_{zz}$ set to considerably high values. By modifying thermal conductivity, a 1D temperature profile along the flow direction was derived

for each fuel channel. The mass flow in each channel was calculated by assuming an equal pressure drop across all the channels. The 3DSTH-MSR used the 3D convection–diffusion equation to calculate the temperature distribution across the entire reactor core of the GMC-MSR. This approach considered thermal coupling between fuel assemblies, as well as the reflector temperature field. In comparison with CFD software, 3DSTH-MSR required fewer computational resources because it only solves one 3D convection–diffusion equation.

The 3DSTH-MSR was constructed on COMSOL Multiphysics and validated against the results from a single-pipe model using RELAP5, demonstrating consistency in temperature predictions under varying energy distributions. The 3DSTH-MSR simulation of 2MW-MSR's steady-state behavior showed that the grid resolution did not significantly affect the maximum and average temperatures as it exceeded 0.82 million. The maximum recorded temperature was 628.7 °C at the radial reflector. Thermal coupling between fuel assemblies is less pronounced, except for those near the radial reflector. The mass flow and outlet temperatures within the 2MW-MSR exhibited a relatively uniform distribution.

**Author contributions** All authors contributed to the study conception and design. Material preparation, data collection, and analysis were performed by Long He, Jia-Jie Shen, and Xiang-Zhou Cai. The first draft of the manuscript was written by Long He, and all authors commented on previous versions of the manuscript. All authors read and approved the final manuscript.

**Data availability** The data that support the findings of this study are openly available in Science Data Bank at https://cstr.cn/31253.11.sciencedb.j00186.00438 and https://doi.org/10.57760/sciencedb.j00186.00438.

## Declarations

**Conflict of interest** Xiang-Zhou Cai is an editorial board member for Nuclear Science and Techniques and was not involved in the editorial review, or the decision to publish this article. All authors declare that there is no conflict of interest.

## References


1. M.W. Rosenthal, P.R. Kasten, R.B. Briggs, Molten-salt reactors-history, status, and potential. Nucl. Appl. Technol. **8**, 107–117 (1970). https://doi.org/10.13182/NT70-A28619
2. R.B. Briggs, Molten-salt reactor program semiannual progress report for period ending January 31, 1964. ORNL-3708 (1964). https://doi.org/10.2172/4676587
3. R.H. Guymon, MSRE design and operations report part VIII: Operating procedures. ORNL-TM-908 (1966). https://doi.org/10.2172/4447572
4. J. Serp, M. Allibert, O. Benes, S. Delpech, The molten salt reactor (MSR) in generation IV: overview and perspectives. Prog. Nucl. Energ. **77**, 308–319 (2014). https://doi.org/10.1016/j.pnucene.2014.02.014
5. M.H. Jiang, H.J. Xu, Z.M. Dai, Advanced fission energy program-TMSR nuclear energy system. Bull. Chin. Acad. Sci. **27**, 366–374 (2012). https://doi.org/10.3969/j.issn.1000-3045.2012.03.016
6. H.J. Xu, Thorium energy and Molten Salt Reactor R &D in China. Thorium Energy for the World, pp. 37–44 (2016) https://doi.org/10.1007/978-3-319-26542-1_6
7. Z.C. Zhang, J.F. Hu, J.G. Chen et al., Influence of thermal neutron scattering effect of Flibe molten salt on neutronic performance of molten salt reactors. Nucl. Tech. **46**, 070605 (2023). https://doi.org/10.11889/j.0253-3219.2023.hjs.46.070605. **(in Chinese)**
8. R.J. Liang, L.J. Sun, X.W. Jiao et al., Reliability analysis and optimization of core fuel salt emergency drain system for the molten salt reactor experiment. Nucl. Tech. **46**, 030604 (2023). https://doi.org/10.11889/j.0253-3219.2023.hjs.46.030604. **(in Chinese)**
9. S.Q. Hu, J. Tian, C. Zhou et al., Optimal design of core flow distribution for 10 MW liquid fuel molten salt reactor. Nucl. Tech. **45**, 110601 (2022). https://doi.org/10.11889/j.0253-3219.2022.hjs.45.110601. **(in Chinese)**
10. J.T. Cao, G.F. Zhu, Z.X. Gu, Influence of core structural changes in dispersed-graphite-component molten salt reactor on nuclear reactivity. Nucl. Tech. **47**, 060601 (2024). https://doi.org/10.11889/j.0253-3219.2024.hjs.47.060601. **(in Chinese)**
11. M.Y. Peng, Y.F. Liu, Y. Zou et al., Characteristics of transuranic nuclides incinerated in a small modular chloride fast reactor. Nucl. Tech. **47**, 020606 (2024). https://doi.org/10.11889/j.0253-3219.2024.hjs.47.020606. **(in Chinese)**
12. R.C. Robertson, Conceptual design study of a single fluid molten-salt breeder reactor. ORNL-4541 (1971). https://doi.org/10.2172/4030941
13. J.R. Engel, P.N. Haubenreich, Temperatures in the MSRE core during steady state power operations. ORNL-TM-738 (1962). https://doi.org/10.2172/4749259
14. D.L. Zhang, S.Z. Qiu, C.L. Liu et al., Steady thermal hydraulic analysis for a molten salt reactor. Nucl. Sci. Tech. **19**, 187–192 (2008). https://doi.org/10.1016/S1001-8042(08)60048-2
15. Z.P. Guo, C.L. Wang, D.L. Zhang et al., The effects of core zoning on optimization of design analysis of molten salt reactor. Nucl. Eng. Des. **256**, 967–977 (2013). https://doi.org/10.1016/j.nucengdes.2013.09.036
16. D. Lecarpentier, V. Carpentier, A neutronic program for critical and nonequilibrium study of mobile fuel reactors: the Cinsf1D code. Nucl. Sci. Eng. **143**, 33–46 (2003). https://doi.org/10.13182/NSE03-A2316
17. W. Yu, R. Jian, L. He et al., Development of TREND dynamics code for molten salt reactors. Nucl. Eng. Technol. **53**, 455–465 (2021). https://doi.org/10.1016/j.net.2020.07.030
18. T. Hanusek, R.M. Juan, Analysis of the power and temperature distribution in molten salt reactors with TRACE. Application to the MSRE. Ann. Nucl. Energy **157**, 108208 (2021). https://doi.org/10.1016/j.anucene.2021.108208
19. Q. Wei, W. Guo, H.L. Wang et al., Develop and verify coupling program of the neutron physics and thermal hydraulic for MSR. Nucl. Tech. **40**, 100605 (2017). https://doi.org/10.11889/j.0253-3219.2017.hjs.40.100605. **(in Chinese)**
20. Y. Cui, L. Cui, S.P. Xia, Dynamic analysis for a 2 MW liquid-fueled molten salt reactor. Prog. Nucl. Energy **126**, 103381 (2020). https://doi.org/10.1016/j.pnucene.2020.103381
21. U. Rohde, S. Kliem, U. Grundmann et al., The reactor dynamics code DYN3D - models, validation and applications. Prog. Nucl. Energy **89**, 170–190 (2016). https://doi.org/10.1016/j.pnucene.2016.02.013
22. K. Zhuang, L.Z. Cao, Y.Q. Zheng et al., Studies on the molten salt reactor: code development and neutronics analysis of MSRE-type design. J. Nucl. Sci. Technol. **52**, 251–263 (2015). https://doi.org/10.1080/00223131.2014.944240

23. K. Zhuang, L.Z. Cao, Numerical analysis on the dynamic behaviors of a graphite-moderated molten salt reactor based on MOREL2.0 code. Ann. Nucl. Energy **117**, 3–11 (2018). https://doi.org/10.1016/j.anucene.2018.02.048
24. X.D. Zuo, M.S. Cheng, Z.M. Dai, Development and validation of a three-dimensional dynamics code for liquid-fueled molten salt reactors. Nuc. Tech. **45**, 030603 (2022). https://doi.org/10.11889/j.0253-3219.2022.hjs.45.030603 **(in Chinese)**
25. Y. Cui, J.G. Chen, M. Dai et al., Development of a steady state analysis code for molten salt reactor based on nodal expansion method. Ann. Nucl. Energy **151**, 107950 (2021). https://doi.org/10.1016/j.anucene.2020.107950
26. S.Y. Si, Q.C. Chen, H. Bei et al., Modeling and simulation of redesigned thorium molten salt reactor. High Power Laser Part. Beams **29**, 016013 (2017). https://doi.org/10.11884/HPLPB201729.160260. **(in Chinese)**
27. L. He, Y.G. Yu, W. Guo, Steady thermal-hydraulic analysis model for graphite-moderated channel type molten salt reactor. Atom. Energy Sci. Technol. **053**, 319–325 (2019). **(in Chinese)**
28. L. He, C.G. Yu, R.M. Ji, Development of a dynamics model for graphite-moderated channel-type molten salt reactor. Nucl. Sci. Tech. **30**, 18 (2019). https://doi.org/10.1007/s41365-018-0541-7
29. J. Kophazi, D. Lathouwers, J.L. Kloosterman, Development of a three-dimensional time-dependent calculation scheme for molten salt reactors and validation of the measurement data of the molten salt reactor experiment. Nucl. Sci. Eng. **163**, 118–131 (2009). https://doi.org/10.13182/NSE163-118
30. A. Lindsay, G. Ridley, A. Rykhlevskii, Introduction to Moltres: An application for simulation of Molten Salt Reactors. Ann. Nucl. Energy **114**, 530–540 (2018). https://doi.org/10.1016/j.anucene.2017.12.025
31. K. Nagy, D. Lathouwers, C.G.A. T'Joen, Steady-state and dynamic behavior of a moderated molten salt reactor. Ann. Nucl. Energy **64**, 365–379 (2014). https://doi.org/10.1016/j.anucene.2013.08.009
32. J. He, X.B. Xia, J. Cai, Temperature field analysis for the main shielding of the 2-MW thorium-based molten salt experimental reactor. Nucl. Tech. **39**, 040601 (2016). https://doi.org/10.11889/j.0253-3219.2016.hjs.39.040601 **(in Chinese)**
33. A. Cammi, V.D. Marcello, L. Luzzi et al., A multi-physics modelling approach to the dynamics of Molten salt reactors. Ann. Nucl. Energy **38**, 1356–1372 (2011). https://doi.org/10.1016/j.anucene.2011.01.037
34. J.W. Cooke, B. Cox, Forced-convection heat-transfer measurements with a molten fluoride mixture flowing in a smooth tube. ORNL-TM-4079 (1973). https://doi.org/10.2172/4486196
35. COMSOL Multiphysics, Introduction to COMSOL multiphysics. (2016)
36. L. He, Development of a steady state and time-dependent coupled neutronics/thermal-hydraulics model and safety characteristics research for the Molten Salt Reactor. Ph.D. Thesis, Shanghai Institute of Applied Physics (2018). **(in Chinese)**
37. Information Systems Laboratories, Inc, RELAP5/MOD3.3 code manual volume 2: user's guide and input requirements (2001)
38. L. He, Y.G. Yu, W. Guo, Development of a coupled code for steady-state analysis of the graphite-moderated channel type molten salt reactor. Sci. Technol. Nucl. Ins. **2018**, 4053254 (2018) https://doi.org/10.1155/2018/4053254
39. ORNL, SCALE: a Modular code system for performing Stan dardized computer analyses for licensing evaluations, ORNL, USA (2005)
40. D.L. Zhang, S.Z. Qiu, G.H. Su, Development of a steady state analysis code for a molten salt reactor. Ann. Nucl. Energy **36**, 590–603 (2009). https://doi.org/10.1016/j.anucene.2009.01.004
41. B. Zhou, R. Yan, Y. Zou et al., Analysis of decay heat in primary loop of molten salt reactor under normal conditions. Nucl. Tech. **41**, 040602 (2018). https://doi.org/10.11889/j.0253-3219.2018.hjs.41.040602